Desalination 568 (2023) 117006

Contents lists available at ScienceDirect

Desalination

journal homepage: www.elsevier.com/locate/desal

The analytic solution of interfacial concentration with observed rejection ratio during dead-end membrane filtration

Albert S. Kim

Civil and Environmental Engineering, University of Hawaii at Manoa, 2540 Dole Street, Holmes 383, Honolulu, HI 96822, United States of America

GRAPHICAL ABSTRACT

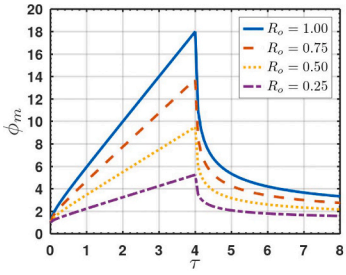

$$\phi_m(\tau \le \tau_s) = 1 + 2R_o\left[\tau + \left(\tau + \tfrac{1}{2}\right)\mathrm{erf}\left(\sqrt{\tau}\right) + \sqrt{\frac{\tau}{\pi}}e^{-\tau}\right]$$

$$\phi_m(\tau_s < \tau) = 1 + \left[\phi_m(\tau_s) - 1\right]e^{\beta^2(\tau-\tau_s)}\,\mathrm{erfc}\left(\beta\sqrt{\tau-\tau_s}\right)$$

Interfacial concentration profiles for constant-flux dead-end filtration, obtained analytically, with various observed rejection ratios

$$R_i \simeq \sqrt{R_o}$$

- The intrinsic rejection ratio can be estimated as a square root of the observed rejection.

ARTICLE INFO

Keywords:
Dead-end filtration
Concentration polarization
Interfacial concentration
Analytic solution
Laplace transform
Robin boundary condition

ABSTRACT

In this study, we revisit the fundamentals of constant–flux dead–end filtration, develop an analytical solution of the interfacial concentration $\phi_m(\tau, R_o)$ as a function of dimensionless time τ and observed rejection R_o, and compare the solution with previous work developed for constant intrinsic rejection, R_i. The excessive concentration, $\phi_m(\tau, R_o) - 1$, consists of three nonlinear terms of τ and reaches $4R_o\tau$ in an asymptotic limit of $\tau > 1/2$. We apply the Robin (mixed) and Dirichlet boundary conditions on the membrane surface and at a far feed–entrance, respectively. The mathematical difficulties for the inverse Laplace transform are resolved using a linear combination of the Laplace transform of error and complementary error functions and applying the convolution theorem. We analytically obtain the unsteady variation of the interfacial concentration after the pressure release using the global mass balance and numerically calculate the required time to reduce the interfacial concentration to a specific limit. More importantly, a relationship between observed and intrinsic rejection ratios is found, such as, $R_o \simeq \sqrt{R_i}$, and verified using experimental data from the literature.

1. Introduction

Membrane separation processes can be conducted in dead-end and crossflow filtration modes. Dead-end filtration involves the feed flow approaching perpendicularly to the membrane surface in a closed container. In contrast, crossflow filtration requires the feed stream to

E-mail address: albertsk@hawaii.edu.
URL: https://www.albertsk.org.

https://doi.org/10.1016/j.desal.2023.117006
Received 12 June 2023; Received in revised form 20 September 2023; Accepted 20 September 2023
Available online 25 September 2023

flow tangentially through the membrane channel. Each mode has unique advantages and disadvantages, and careful consideration should be given to which mode is most appropriate for given purposes. During desalination, solutes are rejected by the membrane, causing a higher surface concentration than the background concentration, such as the feed or initially uniform concentration. The concentration gradient formation is referred to as the concentration polarization (CP) phenomenon, formed within a thin boundary layer above the membrane surface. Fundamental analyses of CP formation and its evolution are essential to ensure the optimal performance of desalination systems [1–3].

Concentration polarization (CP) reduces the driving force for solvent transport through the membrane and gradually decreases solvent recovery and solute rejection. As a reversible fouling phenomenon, CP forms at the beginning of filtration, intensifies proportionally to the produced permeate volume, and disappears when the driving force stops. If the height of the membrane channel is similar to the thickness of CP, the fouling caused by CP can be accelerated because thin membrane channels may increase bulk concentration above the membrane surface from the feed concentration. The CP often triggers irreversible fouling on the membrane surface. The phenomenological significance of the CP resides in various applications and phenomena, such as, but not limited to, battery charging speed [4], patterned surface occurrence [5], mesopores [6], and micro-nanofluidic channels [7]. Given the dynamic existence of the CP layer, visual CP-layer detection can be challenging: however, if realistically implemented, it can significantly contribute to a fundamental understanding of the growth and evolution of the CP phenomena [8–10].

A primary objective of membrane research is to minimize the CP phenomena, necessitating comprehensive experimental, theoretical, and simulational investigations to understand the dynamic characteristics of the CP phenomena. Due to the complex nature of mass and momentum transfer during membrane filtration processes, numerical approaches are often used to solve transport governing equations. Software packages, available in open–source communities and commercial markets, are used to model the filtration phenomena and provide physically meaningful solutions. However, the quantitative numerical results are obtained with input conditions and predetermined parameters during simulations. Sensitivity analyses of numerical solutions often require a series of simulations with various parameter values. On the other hand, theoretical approaches build a simplified model system of target phenomena, employ reasonable assumptions and approximations, and provide analytical solutions for governing equations. The reliability of these models depends on the level of theoretical approximations and, more importantly, the availability of exact analytical solutions to interpret experimental observations.

The governing equation for the mass transport in membrane filtration is classified as a parabolic partial differential equation (PDE), referred to as the convection-diffusion or advection-diffusion equation [11–13]. The main challenge in solving the governing equation stems from the mixed boundary condition (BC) on the membrane surface, also known as the Robin BC [14–16], which balances the convective feed flux toward the membrane surface and the back–diffusion of accumulated solutes within the CP layer. Due to incomplete solute rejection, a fraction of solutes still pass through to the membrane material and provides a non-zero solute concentration in the permeate stream. The Robin boundary condition limits the solute transport through the membrane, and therefore, eliminates the steady state during the dead-end filtration.

In applied and engineering mathematics, the 1D unsteady transport equation often includes diffusion, convection, and reaction. The analytic solutions were obtained using the Laplace transform, or the separation of variables followed by the Fourier transform (only), e.g., for the first–order reaction. The presence of source and sink terms, varying with coordinates and concentration, makes the solving procedure much more difficult. A recent mathematical development provides a general method to obtain 1D steady analytical solutions without the inverse Laplace transform [17]; however, this general solution method is limited to Dirichlet or Neumann BCs by specifying the concentration and its gradient, respectively.

Obtaining analytical solutions using the Laplace transform is limited to cases where their inverse Laplace transform is available by performing the Bromwich integral directly or using prebuilt formulae in mathematical tables. The existing literature includes analytical solutions for heat and diffusion equations only for steady–state convective diffusion or unsteady-state diffusion [11,12], subject to Dirichlet or Neumann boundary conditions. In the dead-end filtration literature, the constant-pressure mode (CPM) has been more actively investigated than the constant-flux mode (CFM), especially for perfect or near-perfect rejection cases. In addition, the governing equation of crossflow filtration is a 2D unsteady parabolic equation, including convection and diffusion in the longitudinal and transverse directions. Analytical solutions for concentration and permeate flux have been obtained [18], assuming a linear shear flow within the CP layer without cake formation. In the theoretical work, the separation of variables method has been utilized to analytically determine a steady–state concentration as a combination of Airy functions [19]. When employing crossflow filtration, the linear shear flow has an insignificant influence on the CP formation during the early stages of the filtration procedure. Therefore, the initial flux decline in cross-flow filtration is comparable to that of dead-end filtration [20,21].

2. Theory

Industrial sectors favor CFM operation, as it facilitates a prescheduled production rate. The hydraulic pressure is automatically regulated to restore the declined flux to the predetermined level, and the recovered flux continues accumulating solute molecules on the membrane surface.

2.1. Governing equation

The governing equation of dead-end filtration [22,23] may be written as

$$\frac{\partial C}{\partial t} = \frac{\partial}{\partial y}\left(D_0\frac{\partial C}{\partial y} + J_w C\right) \tag{1}$$

where $C(t,y)$ is the solute concentration as a function of time t and coordinate y normal to the interface; D_0 is the constant solute diffusivity; and J_w is the uniform permeate flux (in magnitude), defined as the permeated solvent volume per unit time and per unit membrane area. The filtration performance is often measured using the observed rejection ratio, defined as

$$R_o = 1 - \frac{C_p}{C_f} \tag{2}$$

where C_f and C_p are feed and permeate concentrations, respectively; and in a batch operation, C_f also refers to the initial concentration.

We consider the following scenarios for the theoretical development. First, the membrane channel is uniformly filled with the feed solution, C_f, at the beginning of the filtration. Second, the feed–stream of C_f enters the membrane channel sufficiently far from the membrane surface. Third, the convective transport of solutes toward the interface is counter-balanced with solute back–diffusion, resulting in non-zero C_p. The above-mentioned three conditions are written as

$$C(y, t=0) = C_f \tag{3}$$

$$C(y\to\infty, t) = C_f \tag{4}$$

$$D_0\frac{\partial C_m}{\partial y} + J_w C_m = J_w C_p \tag{5}$$

where $C_m = C(t, y = 0)$ is the unsteady interfacial concentration, and

$$\frac{\partial C_m}{\partial y} = \left[\frac{\partial C(y,t)}{\partial y}\right]_{y=0} \tag{6}$$

is its gradient. Eq. (5) is the Robin boundary condition, also called the third or mixed boundary condition, and its physical implications can be found elsewhere [24–26]. The governing Eq. (1) with conditions of Eqs. (3)–(5) is applicable to both CFM and CPM operations with specific dependence of J_w on C_m.

The mass transfer phenomena through nanofiltration or reverse osmosis membranes are often described using the solution–diffusion model [27,28], such as

$$J_w = A(\Delta P - \Delta \Pi_m) \tag{7}$$

$$J_s = B\Delta C_m \tag{8}$$

respectively; where A and B are the solvent and solute permeabilities through the membrane; ΔP is the applied hydraulic pressure; and $\Delta \Pi_m$ and ΔC_m are the transmembrane differences of the osmotic pressure and solute concentration, respectively. In the CPM, ΔP is fixed, and the permeate flux J_w decreases with time due to the unsteady growth of interfacial osmotic pressure $\Delta \Pi_m$. In the CFM, the constant flux J_w is maintained at its initial level throughout the filtration, which requires the continuous growth of hydraulic pressure.

2.2. Nondimensionalization

2.2.1. Representative scale parameters

We scale the concentration C by its representative value of C_f to have a dimensionless concentration ϕ. The dimensionless coordinate η and time τ are defined by dividing the coordinate y and time t by representative length scale L and time scale T, respectively, to be determined later. The dimensionless quantities of ϕ, η, and τ have linear relationships to their real physical quantities, such as

$$C = C_f \phi \tag{9}$$

$$y = L\eta \tag{10}$$

$$t = T\tau \tag{11}$$

that provide the dimensionless form of Eq. (1), such as

$$\frac{\partial \phi}{\partial \tau} = \frac{\partial^2 \phi}{\partial \eta^2} + \mathrm{Pe}\,\lambda \frac{\partial \phi}{\partial \eta} \tag{12}$$

where

$$\mathrm{Pe} = \frac{J_w L}{D_0} (= 2) \tag{13}$$

is the Peclet number, and λ is a controlling parameter used in this study for additional theoretical analyses. Because the selection of L is arbitrary, we assign $\mathrm{Pe} = 2$ in Eq. (13) to have

$$L = \frac{2D_0}{J_w} \tag{14}$$

which automatically determines the time scale parameter, such as

$$T = \frac{L^2}{D_0} = \frac{4D_0}{J_w^2} \tag{15}$$

Most inorganic ions have diffusivity in water of an order of $O(10^{-9})$ m^2/s: for example, the diffusivity of sodium and chloride are 1.334×10^{-9} m^2/s and 2.032×10^{-9} m^2/s, respectively [29]. If we assume that the membrane permeate flux is of an order of 10 $\mathrm{L/m^2\,h}$ [LMH], i.e., 2.7 $\mu\mathrm{m/s}$, scaling parameters are estimated using the sodium diffusivity, such as

$$L = \frac{2D_0}{J_w} = \frac{2\cdot(1\times 10^{-9})}{2.7\times 10^{-6}}\,\mathrm{m} \simeq 1.0\ \mathrm{mm} = O(10^0)\ \mathrm{mm} \tag{16}$$

$$T = \frac{4D_0}{J_w^2} = \frac{4\cdot(1\times 10^{-9})}{(2.7\times 10^{-6})^2}\,\mathrm{s} = 12.20\ min = O(10^1)\ min \tag{17}$$

respectively, where $O(\cdots)$ represents an order of magnitude of a quantity of interest. Note that L and T are estimated as fractions of a millimeter and an hour, respectively.

2.3. Growth of interfacial concentration

2.3.1. Analytic solution

We rewrite the governing equation in a dimensionless form, such as

$$\frac{\partial \phi}{\partial \tau} = \frac{\partial^2 \phi}{\partial \eta^2} + 2\lambda \frac{\partial \phi}{\partial \eta} \tag{18}$$

with the required conditions of

$$\phi(\tau = 0, \eta) = 1 \tag{19}$$

$$\phi(\eta \to \infty, \tau) = 1 \tag{20}$$

$$\frac{\partial \phi_m}{\partial \eta} + 2\lambda(\phi_m - \phi_p) = 0 \tag{21}$$

where $\phi_m(\tau) = C_m(t)/C_f$ and $\phi_p = C_p/C_f = 1 - R_o$ are the dimensionless forms of interfacial and permeate concentrations, respectively, and

$$\frac{\partial \phi_m}{\partial \eta} = \left[\frac{\partial \phi}{\partial \eta}\right]_{\eta=0}$$

is the gradient of ϕ_m at the interface $(\eta = 0)$. As noted above, λ is a parameter to specify the physical characteristics of the convection flow J_w. If $\lambda > 0$, the flow direction is toward the membrane surface in $-y$ direction. If $\lambda < 0$, the flow direction is away from the membrane surface to the bulk phase, representing the backflushing process, which is out of our scope in the current research. Especially, $\lambda = 0$ can represent the sole back-diffusion phenomena when the permeation stops temporarily for membrane cleaning or pressure adjustment.

The theoretical goal of the current work is to calculate the dimensionless, unsteady interfacial concentration $\phi_m(\tau)$ in the CFM. Because L is determined using constant D_0 and J_w, the dimensionless governing Eq. (18) does not include a specific Peclet number. Therefore, each term in the governing equation is properly balanced in magnitude, which is advantageous in obtaining reliable numerical solutions later. We restrict ourselves to $\lambda = +1$ to investigate the transient build-up of the interfacial concentration $\phi_m(\tau)$, which determines the instantaneous pressure growth for the constant J_w.

The Laplace transform for $\phi(\tau, \eta)$ is defined, such as

$$\mathscr{L}[\phi(\tau,\eta)] = \Phi(p,\eta) = \int_0^\infty e^{-p\tau}\phi(\tau,\eta)\mathrm{d}\tau \tag{22}$$

which gives

$$\mathscr{L}\left[\frac{\partial \phi}{\partial \tau}\right] = p\Phi - \phi(\eta, \tau = 0) \tag{23}$$

$$\mathscr{L}\left[\frac{\partial \phi}{\partial \eta}\right] = \frac{\partial \Phi}{\partial \eta} \tag{24}$$

$$\mathscr{L}\left[\frac{\partial^2 \phi}{\partial \eta^2}\right] = \frac{\partial^2 \Phi}{\partial \eta^2} \tag{25}$$

where $\phi(\eta, \tau = 0) = 1$ is the initial uniform concentration. Substitution

of Eqs. (23)–(25) into Laplace-transformed (18) gives

$$\frac{\partial^2\Phi}{\partial\eta^2}+2\frac{\partial\Phi}{\partial\eta}-p\Phi=-1 \tag{26}$$

of which the general solution is

$$\Phi(p,\eta)=\frac{1}{p}+e^{-\eta}(C_1e^{-\alpha\eta}+C_2e^{+\alpha\eta}) \tag{27}$$

where $\alpha=\sqrt{1+p}$ for $p>0$, and C_1 and C_2 are unknown integration constants. A derivative of Eq. (27) is calculated, such as

$$\frac{\partial\Phi}{\partial\eta}=-(\alpha+1)C_1e^{-(\alpha+1)\eta}+C_2(\alpha-1)e^{(\alpha-1)\eta} \tag{28}$$

Note that the initial condition of Eq. (19) is already applied during the Laplace transform process. Now, we determine two unknown constants in Eq. (28). First, Φ of Eq. (27) should be finite within the spatial domain of $0<\eta<\infty$, so we let $C_2=0$ and avoid the divergence of Φ at $\eta\to\infty$. Second, we calculate the Laplace transform of the interfacial condition of Eq. (21), such as

$$\frac{\partial\Phi_m}{\partial\eta}+2\Phi_m=2\frac{1-R_o}{p} \tag{29}$$

and substitute Eqs. (27) and (28) into Eq. (29) to determine

$$C_1=\frac{2R_o}{p(\sqrt{1+p}-1)} \tag{30}$$

The Laplace transform of the far–field boundary condition of Eq. (20) is straightforward, such as

$$\lim_{\eta\to\infty}\Phi=\frac{1}{p} \tag{31}$$

Finally, we obtain the specific Φ that satisfies the three required conditions, such as

$$\Phi=\frac{1}{p}+2R_o\cdot K(p)e^{-\left(1+\sqrt{1+p}\right)\eta} \tag{32}$$

where

$$K(p)=\frac{1}{p(\sqrt{1+p}-1)} \tag{33}$$

which includes the transient behavior of the excessive interfacial concentration at $\eta=0$. An inverse Laplace transform Φ of Eq. (32) provides the complete analytic solution for the unsteady concentration profile at time τ in the full space domain, which requires the Bromwich integral, such as

$$\begin{aligned}\phi(\tau,\eta)&=1+2R_o\mathscr{L}^{-1}\left[K(p)e^{-\left(1+\sqrt{1+z}\right)\eta}\right]\\&=1+\frac{2R_o}{2\pi i}\oint dz e^{z\tau}K(z)e^{-\left(1+\sqrt{1+z}\right)\eta}\end{aligned} \tag{34}$$

where the real parameter p is replaced by a complex variable z. Due to the term containing $\sqrt{z+1}$, the direct integral of Eq. (34) is challenging, and moreover, $L^{-1}[K(z)]$ is not currently found in mathematical tables.

We focus on the transient interfacial concentration at $\eta=0$, such as

$$\phi_m(\tau)=1+2R_o\mathscr{L}^{-1}[K(p)] \tag{35}$$

to calculate the $\mathscr{L}^{-1}[K(p)]$ by taking the following steps. First, we multiply $\sqrt{p+1}+1$ by the numerator and denominator of K to rewrite it, such as

$$K(p)=\frac{1+\sqrt{p+1}}{p^2}=K_1(p)+K_2(p) \tag{36}$$

where

$$K_1(p)=\frac{1}{p^2} \tag{37}$$

$$K_2(p)=\frac{\sqrt{p+1}}{p^2} \tag{38}$$

The inverse Laplace transform of K_1 is straightforward, such as

$$\mathscr{L}^{-1}[K_1]=\tau \tag{39}$$

and that of K_2 requires some extra steps to apply the convolution theorem. We reformulate K_2 as a product of $F(p)$ and $G(p)$, such as

$$K_2(p)=F(p)G(p) \tag{40}$$

where

$$F(p)=\frac{1}{p} \tag{41}$$

$$G(p)=\frac{\sqrt{p+1}}{p} \tag{42}$$

and use the following Laplace transform formulae [30], such as

$$\mathscr{L}\left[erfc\left(-\sqrt{\tau}\right)\right]=\frac{\sqrt{p+1}+1}{p\sqrt{p+1}}=\frac{1}{p}+\frac{1}{p\sqrt{p+1}} \tag{43}$$

$$\mathscr{L}\left[erfc\left(+\sqrt{\tau}\right)\right]=\frac{\sqrt{p+1}-1}{p\sqrt{p+1}}=\frac{1}{p}-\frac{1}{p\sqrt{p+1}} \tag{44}$$

where erfc is the complementary error function, defined as

$$erfc(z)=1-erf(z)=\frac{2}{\sqrt{\pi}}\int_z^\infty e^{-y^2}\mathrm{d}y \tag{45}$$

and the original error function is

$$erf(z)=\frac{2}{\sqrt{\pi}}\int_0^z e^{-y^2}\mathrm{d}y \tag{46}$$

For simplicity, we define

$$\mathscr{L}\left[erfc\left(-\sqrt{\tau}\right)\right]=L_- \tag{47}$$

$$\mathscr{L}\left[erfc\left(+\sqrt{\tau}\right)\right]=L_+ \tag{48}$$

and rewrite $G(p)$ such as

$$G(p)=\frac{1}{2}(L_--L_+)+\frac{1}{\sqrt{p+1}} \tag{49}$$

Then, we calculate the inverse Laplace transform of $G(p)$, such as

$$\mathscr{L}^{-1}[G(p)]=\frac{1}{2}\mathscr{L}^{-1}[(L_--L_+)]+\mathscr{L}^{-1}\left[\frac{1}{\sqrt{p+1}}\right] \tag{50}$$

$$=erf\left(\sqrt{\tau}\right)+\frac{e^{-\tau}}{\sqrt{\pi\tau}} \tag{51}$$

and rewrite $\mathscr{L}^{-1}[K_2(p)]$, such as

$$\mathscr{L}^{-1}[K_2(p)]=\mathscr{L}^{-1}[F(p)G(p)]=f^*g=g^*f \tag{52}$$

where $f(\tau)$ and $g(\tau)$ are the inverse Laplace transform of $F(p)$ and $G(p)$, respectively, such as

$$f(\tau)=\mathscr{L}^{-1}[F(p)]=1 \tag{53}$$

$$g(\tau)=\mathscr{L}^{-1}[G(p)]=erf\left(\sqrt{\tau}\right)+\frac{e^{-\tau}}{\sqrt{\pi\tau}} \tag{54}$$

In Eq. (52), operator * indicates the convolution integrals, such as

$$f^{*}g = \int_0^{\tau} f(\tau - x)\, g(x)\mathrm{d}x \tag{55}$$

$$g^{*}f = \int_0^{\tau} g(\tau - x) f(x)\mathrm{d}x \tag{56}$$

To take advantage of the constant function $f(x) = 1$, we choose Eq. (55), such as

$$f^{*}g = \int_0^{\tau} \mathrm{d}x \cdot 1 \cdot \left(erf\left(\sqrt{x}\right) + \frac{e^{-x}}{\sqrt{\pi x}} \right) \tag{57}$$

$$= \left(\tau + \frac{1}{2}\right) erf\left(\sqrt{\tau}\right) + \sqrt{\frac{\tau}{\pi}} e^{-\tau} \tag{58}$$

We finally obtain the analytical representation of the unsteady interfacial concentration in the CFM, such as

$$\phi_m(\tau) = 1 + 2R_o \left[\tau + \left(\tau + \frac{1}{2}\right) erf\left(\sqrt{\tau}\right) + \sqrt{\frac{\tau}{\pi}} e^{-\tau} \right] \tag{59}$$

indicating that the excessive concentration, i.e., $\phi_m - 1$ is linear to the observed rejection ratio, R_o. Special cases of Eq. (59) include the zero and perfect rejection cases, such as

$$\lim_{R_o \to 0} \phi_m(\tau) = 1 \tag{60}$$

and

$$\lim_{R_o \to 1} \phi_m(\tau) = (1 + 2\tau)\left[1 + erf\left(\sqrt{\tau}\right)\right] + 2\sqrt{\frac{\tau}{\pi}} e^{-\tau} \tag{61}$$

respectively. Note that $erf(x)$ increases monotonously when τ increases from 0 to 1, and afterward reaches a plateau value of 1 gradually, having a similar shape to the hyperbolic tangent function [31]. See Appendix A.1 for details.

2.3.2. Numerical solutions

Numerical solutions are often obtained to understand complex phenomena when analytical solutions are challenging. On the other hand, numerical solutions can be used to cross–validate theory–oriented analytical solutions. Among multiple numerical schemes available to solve the PDE, we employ the forward, explicit scheme to monitor numerical errors sensitive to intervals.

The dimensionless concentration $\phi(\tau, \eta)$ is discretized, such as $\phi_{j,k}$ for τ–index $j = 1 - M$ and η–index $k = 1 - N$. The time and length intervals of $\delta\tau$ and $\delta\eta$ are determined, such as

$$\delta\tau = \frac{\tau_{\max}}{M} \quad \text{and} \quad \delta\eta = \frac{\eta_{\max}}{M} \tag{62}$$

respectively, where $\tau_{\max}$ and $\eta_{\max}$ are the time and spatial maxima, respectively. Because the interfacial condition of Eq. (21) includes $\partial\phi/\partial\eta$, the interfacial concentration, $\phi_m(\tau) = \phi_{j1}$, should be calculated using its neighbors in the computational grid. In this study, we test the differentiation schemes using 2, 3, and 5 points, such as

$$\phi_{j1}^{[2]} = \frac{\phi_{j2} - \lambda\phi_p\delta\eta}{(1 - \lambda\delta\eta)} \tag{63}$$

$$\phi_{j,1}^{[3]} = \frac{4\phi_{j2} - \phi_{j3} - 2\lambda\phi_p\delta\eta}{(3 - 2\lambda\delta\eta)} \tag{64}$$

$$\phi_{j,1}^{[5]} = \frac{48\phi_{j2} - 36\phi_{j3} + 16\phi_{j4} - 3\phi_{j5} - 12\lambda\phi_p\delta\eta}{(25 - 12\lambda\delta\eta)} \tag{65}$$

and discuss their sensitivity analyses in the next section. Detailed procedures for the numerical solutions are in Appendix A.2.

2.4. Decline of interfacial concentration after pressure release

The dead–end filtration at the CFM is designed to periodically stop whenever the hydraulic pressure exceeds a predetermined limit. The unsteady declining behavior of the interfacial concentration after the pressure release can be modeled by solving the governing Eq. (12) with $\lambda = 0$, such as

$$\frac{\partial\phi}{\partial\tau} = \frac{\partial^2\phi}{\partial\eta^2} \quad \text{for} \quad \tau \geq \tau_s \tag{66}$$

where τ_s is the specific time when the hydraulic pressure is released. In this specific case, the far–field boundary condition is kept valid, regardless of λ, such as

$$\phi(\eta \to \infty, \tau \geq \tau_s) = 1 \tag{67}$$

but the interfacial condition is changed to the Neumann boundary condition, such as

$$\left[\frac{\partial\phi_m}{\partial\eta}\right]_{\eta=0} = 0 \tag{68}$$

When the permeation stops at $\tau = \tau_s$, the spatial variation of $\phi(\eta, \tau_s)$ becomes an initial condition for the subsequent back-diffusion phenomena, denoted as

$$\phi(\tau_s, \eta) = \mu(\eta) \tag{69}$$

which is analytically unknown due to the lack of a full solution for Eq. (34). We take the asymptotic limit of $\mu(\eta)$ to assume

$$\mu(\eta) = 1 + (\phi_{\max} - 1)e^{-\beta\eta} \tag{70}$$

where $\phi_{\max} = \phi_m(\tau_s)$ is the interfacial concentration at $\tau = \tau_s$, and β is a constant to be determined. The global mass balance is written, such as

$$\int_0^{\infty} \left[C(y, t_s) - C_f\right] \mathrm{d}y = \int_0^{t_s} J_w C_f R_o \,\mathrm{d}t \tag{71}$$

where $t_s = T\tau_s$ is the real-time when the filtration stops. The left–hand side of Eq. (71) represents the excessive solute mass retained per unit membrane area at t_s, and its right–hand side indicates the total solute mass retained until $\tau = \tau_s$. We substitute Eq. (70) into Eq. (71) to have

$$\int_0^{\infty} \left[(\phi_{\max} - 1)e^{-\beta\eta}\right] \mathrm{d}\eta = 2R_o\tau \tag{72}$$

which gives

$$\beta = \frac{(\phi_{\max} - 1)}{2R_o\tau} \tag{73}$$

To obtain constant β, we take its asymptotic limit at $\tau \gg 1/2$ by using the limiting values of $erf\left(\sqrt{\tau}\right) \to 1$, $e^{-\tau} \to 0$, and $\phi_{\max} - 1 \simeq 4R_o\tau$ to obtain

$$\lim_{1/2 \ll \tau} \beta = \lim_{1/2 \ll \tau} \frac{\phi_{\max} - 1}{2R_o\tau} \to 2 \tag{74}$$

The symbol β is kept during subsequent derivations (instead of using its value 2) to investigate its impact on the concentration profile.

The Laplace transform of the governing Eq. (66) provides

$$\frac{d^2\Phi}{d\eta^2} - p\Phi = -\mu(\eta) \tag{75}$$

whose general solution is

$$\Phi = \frac{1}{p} + C_3 e^{-q\eta} + C_4 e^{+q\eta} + \frac{\phi_{\max} - 1}{q^2 - \beta^2} e^{-\beta\eta} \tag{76}$$

where $q = \sqrt{p}$, and C_3 and C_4 are unknown constants to be determined.

The far-field boundary condition should prevent Φ diverging at $\eta \to \infty$, so we set $C_4 = 0$. The interfacial Dirichlet condition of Eq. (68) gives

$$C_1 = -\frac{(\phi_{\max} - 1)}{q^2 - \beta^2}\frac{\beta}{q} \tag{77}$$

Then, the interfacial Φ at $\eta = 0$ after the pressure release is denoted as Φ_s and obtained, such as

$$\Phi_s(p) = \frac{1}{p} + \frac{(\phi_{\max} - 1)}{q(q+\beta)} \tag{78}$$

and its inverse Laplace transform gives the interfacial concentration after the pressure is released, such as

$$\phi_s(\tau) = \varphi(\Delta\tau) H(\Delta\tau) \tag{79}$$

where $\Delta\tau = \tau - \tau_s$ is the time elapsed after the stopping time τ_s and

$$\varphi(\Delta\tau) = 1 + (\phi_{\max} - 1) e^{\beta^2 \Delta\tau} erfc\left(\beta\sqrt{\Delta\tau}\right) \tag{80}$$

for $\Delta\tau > 0$ and

$$H(\Delta\tau) = \begin{pmatrix} 1 & \text{for} \quad \Delta\tau > 0 \\ 0 & \text{for} \quad \Delta\tau \le 0 \end{pmatrix} \tag{81}$$

is the Heaviside step function. In Eq. (80), the $erfc(x)$ function, defined in Eq. (45), decreases much faster than e^{x^2}, where $x = \beta\sqrt{\Delta\tau}$.

If a specific value of $\varphi(\Delta\tau)$ after τ_s, denoted as $\phi_{\lim}$, is given between $\phi_{\max}$ and 1, Eq. (80) can be solved for $\Delta\tau$, i.e., the dimensionless duration for the interfacial concentration decreases from $\phi_{\max}$ to $\phi_{\lim}$. To estimate the decreasing rate of φ at $\Delta\tau = 0$, we calculate

$$\left[\frac{\partial\varphi}{\partial\Delta\tau}\right]_{\Delta\tau=0} = \lim_{x\to 0}\left[\beta^2 erfc\left(\beta\sqrt{x'}\right) e^{\beta^2 x} - \frac{\beta}{\sqrt{\pi x'}}\right] = -\infty \tag{82}$$

where x' is a dummy variable for the differentiation. Eq. (82) provides the initial rate of the interfacial concentration at the beginning of the pressure release. The negative sign indicates $\varphi(\Delta\tau)$ rapidly decreases with time $\Delta\tau(\rangle 0)$, but the infinite magnitude is physically questionable. The presence of β indicates that the mathematical singularity may originate from our assumption of the exponential concentration profile with η within the CP layer. On the other hand, it is worth noting that $\dot{\varphi}$ is a sole function of the difference $\Delta\tau$, being independent of τ_s.

2.5. Comparison to the previous analytical work

Dresner [22] uses the constant permeate flux, denoted as v_0, to propose dimensionless quantities, including excessive concentration $\Gamma(\tau^*, \eta) = C(\tau^*, \eta)/C_f - 1$, coordinate $\eta^* = v_0 y/D_0 (= 2\eta)$, and time $\tau^* = v_0^2 t/D_0 (= 4\tau)$, where C_f is the initial concentration within a batch experimental cell. The Green function is used to solve for the interfacial concentration with respect to $\{\eta^*, \tau^*\}$ only for the perfect rejection, i.e., $C_p = 0$, such as

$$\psi_m(\tau) = (1 + 2\tau)\left[1 + erf\left(\sqrt{\tau}\right)\right] + 2\sqrt{\frac{\tau}{\pi}} e^{-\tau} \tag{83}$$

where $\tau = \tau^*/4$. Eq. (83) requires subsequent transforms of functions including $\sqrt{p+\lambda}$ where $\lambda = 1/2$. Dresner's $\{\eta^*, \tau^*\}$ and our $\{\eta, \tau\}$ sets can be generally written using $\lambda = 1/2$ and $\lambda = 1$ in Eq. (12), respectively. It is more intuitive to understand physical phenomena using $\{\eta^*, \tau^*\}$, but the $\{\eta, \tau\}$ set generates a convenient mathematical representation in the term of $\sqrt{p+1}$.

The subsequent dead-end filtration theories for the CFM [23] and the CPM [32–34] employ the intrinsic rejection coefficient, defined as

$$R_i = 1 - \frac{C_p}{C_m} \tag{84}$$

which is assumed to be constant during the dead-end filtration. In the previous work, the interfacial excessive concentration has been denoted as $\Gamma_m(\tau^*) = C_m(\tau^*)/C_f - 1$, and we further show its relationship with R_o and R_i, such as

$$\Gamma_m = \frac{R_i - R_o}{1 - R_i} \tag{85}$$

where $R_0 < R_i < 1$ in principle, and therefore

$$\phi_m = \psi_m = \frac{C_m}{C_f} = \frac{1 - R_o}{1 - R_i} > 1 \tag{86}$$

For simplicity, we denote the dimensionless interfacial concentration of the CPM as $\psi_m = \Gamma_m(\tau^*) + 1$ and represent it as a function of τ (instead of τ^*). For example, if R_i is a midpoint value between R_o and 1, i.e., $R_i = (1 + R_o)/2$, then $\Gamma_m = 1$, indicating the interfacial concentration is a double the background concentration, i.e., $\psi_m = 2$. Raridon et al. [23] extend Dresner's work to calculate $\psi_m(\tau)$ of an imperfect intrinsic rejection, such as

$$\psi_{m0}(\tau) = \frac{1}{(1 - R_i)}\left[1 + \frac{1}{2}(1 - 2R_i) e^{-4\tau R_i(1-R_i)} erfc\left[(1 - 2R_i)\sqrt{\tau}\right] - \frac{1}{2} erfc\left(\sqrt{\tau}\right)\right] \tag{87}$$

for $0 < R_i < 1/2$ and

$$\psi_{m1}(\tau) = \frac{1}{1 - R_i}\left[1 - (2R_i - 1) e^{-4\tau R_i(1-R_i)}\right] + \frac{1}{2(1 - R_i)}\left[(2R_i - 1) e^{-4\tau R_i(1-R_i)} erfc\left[(2R_i - 1)\sqrt{\tau}\right] - erfc\left(\sqrt{\tau}\right)\right] \tag{88}$$

for $1/2 < R_i \le 1$. Eq. (88) is not intuitively understood for the perfect intrinsic rejection limit of $R_i \to 1$. Therefore, we additionally calculate the limiting expressions of Eqs. (87) and (88), such as, for $R_i \to 0^+$

$$\psi_{m0}(\tau, R_i \to 0^+) \simeq 1 + 2R_i\left[\sqrt{\frac{\tau}{\pi}} e^{-\tau} - (1 + 2\tau) erfc\left[\sqrt{\tau}\right]\right] \tag{89}$$

and for $R_i \to 1^-$

$$\psi_{m1}(\tau, R_i \to 1^-) = \left(1 + 2R_i^2\tau\right)\left[1 + erf\left(\sqrt{\tau}\right)\right] + 2\sqrt{\frac{\tau}{\pi}} e^{-\tau} \tag{90}$$

respectively. Eq. (89) indicates that the excessive concentration ψ_m is linear to R_i for $R_i \simeq R_o \to 0$. Eq. (90) confirms the theoretical convergence of ψ_{m1} to Dresner's original work of Eq. (83), as well as our analytic solution of Eq. (59) for the perfect rejection of the CFM, i.e., $R_o \to R_i \to 1$.

Now, we calculate the difference between ϕ_m and ψ_{m1} for high rejection, which should converge to zero for large $\tau(\rangle 1)$, such as

$$\phi_m - \psi_m \simeq 4\left(R_o - R_i^2\right)\tau \to 0 \tag{91}$$

because ϕ_m and ψ_m are indicated identically in Eq. (86). Eq. (91) estimates the intrinsic rejection in terms of the observed rejection, such as

$$R_i \simeq \sqrt{R_o} \tag{92}$$

and the interfacial concentration, such as

$$C_m = \frac{C_p}{1 - \sqrt{R_o}} = C_f \frac{1 - R_o}{1 - \sqrt{R_o}} \tag{93}$$

Eq. (93) demonstrates that the interfacial concentration C_m reaches $2C_f$ for a high observed rejection (i.e., $R_o \to 1$), proven as follows, using L'Hôpital's rule [19], such as

$$\lim_{R_o\to 1} C_m = \lim_{R_o\to 1} C_f \frac{1 - R_o}{1 - \sqrt{R_o}} = \lim_{R_o\to 1} C_f \frac{-1}{-\frac{1}{2} R_o^{-1/2}} = 2C_f \tag{94}$$

which is generally unacceptable for NF and RO processes. This theoretical restriction must originate from the basic definition of R_i in Eq. (84) that compels the linear relationship of C_p with transient C_m, even if both change with time. Bouranene et al. [35] report an experimental study on removing cobalt and lead ions from wastewater using polyamide NF membranes. The observed rejection R_o is compared with R_i estimated using the standard film theory. Their experimental observations include $R_o \simeq 0.64$ and $R_i \simeq 0.82$ for two cases of removing glucose solution of 2 g/L and cobalt solution of 0.1 g/L. (See Figs. 3 and 5 of Ref. [35].) Their rejection values support the theoretical approximation of Eq. (92) well, such as $R_i/\sqrt{R_o} = 0.82/\sqrt{0.64} \simeq 1.025$, close to 1. Direct and instantaneous measurements of the interfacial concentration C_m are still challenging, but essential because novel quantitative methods may quantify the intrinsic rejection without employing specific transport models [8].

2.6. Components of interfacial concentration

To investigate the unsteady behavior, we divide the full analytic solution $\phi_m(\tau)$ of Eq. (59) into four component functions, such as

$$\phi_{m0} = 1 \tag{95}$$

$$\phi_{m1} = 2R_o \cdot \tau \tag{96}$$

$$\phi_{m2} = 2R_o \cdot \left(\tau + \frac{1}{2}\right) erf\left(\sqrt{\tau}\right) \tag{97}$$

$$\phi_{m3} = 2R_o \cdot \sqrt{\frac{\tau}{\pi}} e^{-\tau} \tag{98}$$

as shown in Fig. 1, where $\phi_m(\tau) = \phi_{m0} + \phi_{m1} + \phi_{m2} + \phi_{m3}$.

Basically, $\phi_{m0} = 1$ is the constant feed concentration C_f as the background or reference concentration at arbitrary time τ and coordinate η, and therefore, ϕ_{m0} is the only term independent of the rejection ratio R_o. The trivial case is the zero-rejection of $R_o = 0$, which gives $\phi_m = \phi_{m0} = 1$, referring to the absence or failure of the membrane. The first non–trivial function, $\phi_{m1} = 2R_o\tau$, is linear with τ, obtained from $\mathscr{L}^{-1}[K_1(p)]$. ϕ_{m1} indicates the solute accumulation at the interface is linearly proportional to the accumulated filtered volume. The next component functions are ϕ_{m2} and ϕ_{m3}, originating from $\mathscr{L}^{-1}[K_2(p)]$. The stiff increase of ϕ_{m2} for small τ is ascribed to the nonlinear dependence of the error function: in comparison to $erf(\tau)$, $erf\left(\sqrt{\tau}\right)$ increases with τ faster and converges to the plateau value of 1 more slowly. $\tau erf\left(\sqrt{\tau}\right)$ in ϕ_{m2} is ascribed to the initial rapid onset, followed by a linear increase of the interfacial concentration. For $\tau > 1$, indicating that the real-time t is longer than the representative time scale $T\left(= 4D_0/J_w^2\right)$, the effect of the error function, $erf\left(\sqrt{\tau}\right)$, becomes insignificant as it converges to $erf\left(\sqrt{\tau} > 1\right) \to 1$. Similarly, ϕ_{m3} initially increases with $\sqrt{\tau}$ until the exponential term $e^{-\tau}$ becomes significant enough to hinder the gradually increasing trend of $\sqrt{\tau}$. Because ϕ_{m3} is a product of $\sqrt{\tau}$ and $e^{-\tau}$, it has a peak, found at $\tau = \frac{1}{2}$, as shown in the insert of Fig. 1, and the peak value is

$$\phi_{m3}\left(\tau = \frac{1}{2}\right) = [2R_o]_{R_o=1} \cdot 0.2420 \to 0.4839 \tag{99}$$

For a large τ, the asymptotic form of ϕ_m is obtained as

$$\phi^* = \lim_{\tau\to\infty} \phi_m = \lim_{\tau\to\infty} \sum_{k=0}^{3} \phi_{mk} = 1 + R_o(1 + 4\tau) \tag{100}$$

which seems to be valid for $\tau > 0.5$, as visually investigated in Fig. 1. At $\tau = 0.25$, the ratio of the asymptotic form, ϕ_m^*, to the exact form, ϕ_m, is calculated as

$$\frac{\phi^*(\tau = 0.25)}{\phi_m(\tau = 0.25)} = \frac{3.000}{2.672} = 1.123 \tag{101}$$

indicating a 12.3 % error, which will be reduced for a larger τ.

2.7. Evaluation of the interface concentration

Because the unsteady convection-diffusion equation is a parabolic PDE, time and spatial intervals should meet the specific criteria of the numerical schemes used. The time step should be short enough to avoid numerical instability but long enough to calculate the solution within reasonable computing time. The space step should be small enough not to accumulate errors created by calculating gradients.

Using the standard numerical scheme discussed above, we numerically calculate the interfacial concentration $\phi_m(\tau)$ using 2–, 3–, and 5–point differential schemes, denoted as $\phi_m^{[2]}$, $\phi_m^{[3]}$, and $\phi_m^{[5]}$ in Eqs. (A.7)–(A.9) and calculate their error ratios to the exact $\phi_m(\tau)$, defined as

$$f_m^{[k]} = \frac{\phi_m^{[k]}}{\phi_m(\tau)} - 1 \tag{102}$$

where k is 2, 3, and 5. Fig. 2 shows the percentage errors the three

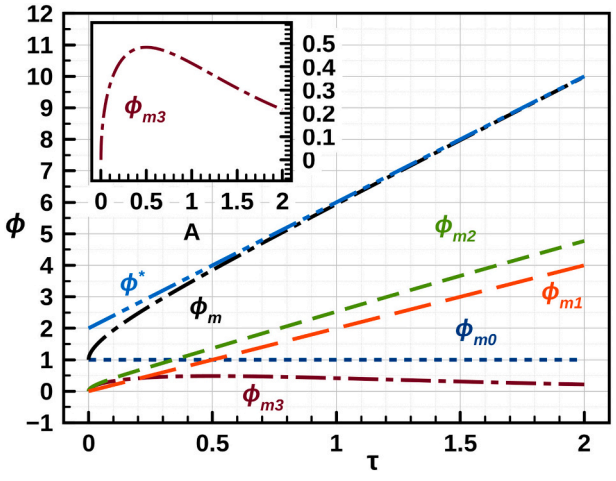

Fig. 1. The interfacial concentration (a) $\phi_m(\tau)$ and its three components: ϕ_{m0}, ϕ_{m1}, ϕ_{m2}, and ϕ_{m3}; and (b) the curvature of $\phi_{m3}(\tau)$ at the peak value of $\phi_{m3}(\tau = 0.5) = 0.4839$ for $R_o = 1$.

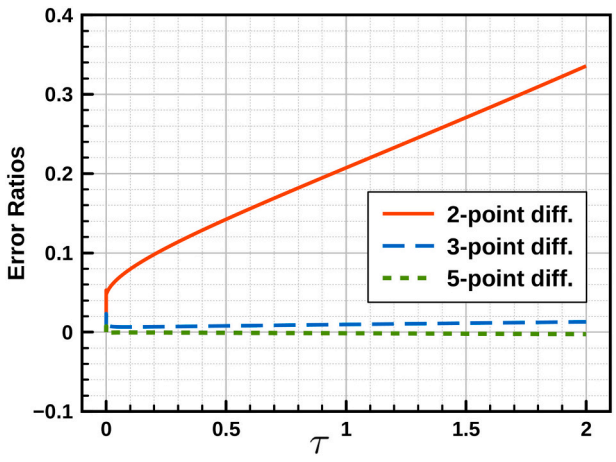

Fig. 2. Percent errors of the 2, 3, and 5–point differential schemes of Eqs. (63), (64), and (65), respectively.

numerical schemes create. In the entire time domain of the current study, i.e., $0 < \tau < 2$, the 5-point differential scheme provides almost identical results to those the analytic solution obtains. The 3-point scheme shows a seemingly linear increase in the error ratio, but the magnitude of errors within the time domain is insignificant. On the other hand, the 2-point scheme shows unacceptable error ranges even in the initial period of $\tau \leq 0.2$, at which the errors exceed 10 %.

2.8. Rate of the interfacial concentration

Besides the transient behavior of $\phi_m(\tau)$, its initial increase rate is of great interest for evaluating the initial pressure growth. We define the rate of ϕ_m, such as

$$\dot{\phi}_m = \frac{\mathrm{d}\phi_m(\tau)}{\mathrm{d}\tau} \tag{103}$$

calculate the rate for each component function, such as

$$\dot{\phi}_{m0} = 0 \tag{104}$$

$$\dot{\phi}_{m1} = 2R_o \cdot 1 \tag{105}$$

$$\dot{\phi}_{m2} = 2R_o \cdot \left[erf\left(\sqrt{\tau}\right) + \left(\frac{1}{2} + \tau\right) \frac{e^{-\tau}}{\sqrt{\pi\tau}} \right] \tag{106}$$

$$\dot{\phi}_{m3} = 2R_o \cdot \left[\left(\frac{1}{2} - \tau\right) \frac{1}{\sqrt{\pi\tau}} e^{-\tau} \right] \tag{107}$$

and obtain their sum, such as

$$\dot{\phi}_m = 2R_o \left(1 + erf\left(\sqrt{\tau}\right) + \frac{e^{-\tau}}{\sqrt{\pi\tau}} \right) \tag{108}$$

as shown in Fig. 3 for an exemplary case of the perfect rejection $R_o = 1$. The second term in the parenthesis on the right–hand side of Eq. (108) is from $\phi_{m2}(\tau)$, and the third term is from both $\phi_{m2}(\tau)$ and $\phi_{m3}(\tau)$. The function $erf\left(\sqrt{\tau}\right)$ has the converging characteristics of $erf(0) \to 0$ and $erf(\infty) \to 1$, and so the second term, including $erf\left(\sqrt{\tau}\right)$, in Eq. (108) contributes to the initial monotonous increase in ϕ_m. (See Appendix A.1 for the mathematical details of the error function and its alternative for numerical evaluation.) Note that $\dot{\phi}_m$ diverges at $\tau = 0$, at which we apply the initial condition, but the real phenomena start at $\tau = 0^+$. Besides, $\dot{\phi}_m$ rapidly decreases until $\tau \simeq 0.2$ and begins to reach its plateau value $4R_0$ around $\tau = 0.5$, at which ϕ_{m3} reaches its maximum. Mathematical representations of the short– and long–term behavior of $\dot{\phi}_m(\tau)$ can be summarized, such as

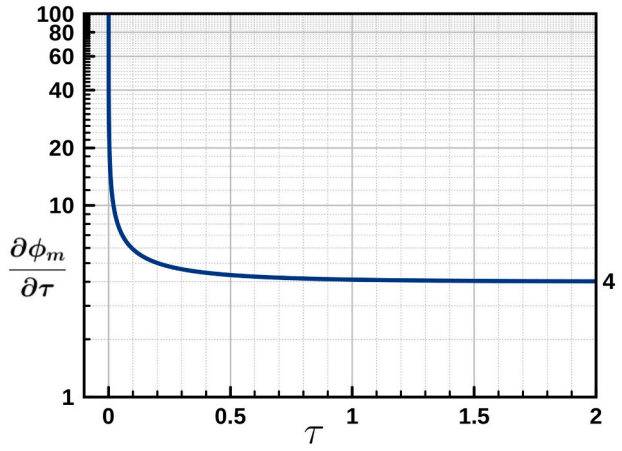

Fig. 3. Rate of $\phi_m(\tau)$, i.e., $\dot{\phi}_m(\tau)$ with respect to τ for $R_o = 1$..

$$\lim_{\tau \to 0} \dot{\phi}_m \simeq \lim_{\tau \to 0} \dot{\phi}_{m3} = \infty \tag{109}$$

$$\lim_{\tau \to \infty} \dot{\phi}_m \simeq \lim_{\tau \to 0} \left(\dot{\phi}_{m1} + \dot{\phi}_{m2} \right) = 4R_o \tag{110}$$

respectively. The convergence of $\dot{\phi}_m$ for a large τ, i.e., specifically $\tau > 2$ and conceptually $\tau \to \infty$, implies the hydraulic pressure ΔP needs to increase proportionally with time, i.e., $\Delta P \propto \phi_m(\tau) \propto \tau$, to maintain the constant flux J_w.

2.9. Effects of rejection ratio

Fig. 4 shows the variation of $\phi_m(\tau, R_o)$ with respect to dimensionless time τ for various rejection ratio values from 0.2 to 1.0. The nonlinear dependence of ϕ_m on τ starts disappearing as τ passes 0.5 for the perfect rejection $(R_o = 1)$. At lower rejection values, the convergence of the exact $\phi_m(\tau)$ to the asymptotic limit occurs at an earlier τ than that for $R_o = 1$. Visual investigation of Fig. 4 indicates that at $\tau \geq 1$, i.e., $t \geq T = O(10)$ *min*, Eq. (100) is an excellent approximation.

Fig. 5 shows the difference between the asymptotic limit $\phi^*(\tau)$ and the exact solution of $\phi_m(\tau)$ for the wide range of τ, i.e., $\phi^*(\tau) - \phi_m(\tau)$, in a logarithm scale. The non–linearity of $\phi_m(\tau)$ starts disappearing at $\tau = 0.5$, as previously indicated in Fig. 4, and the difference becomes negligible before τ reaches 1.0, where the maximum difference falls below 10 %. On the other hand, one can interpret $\phi_m(\tau) - \phi^*(\tau)$ as extra hydraulic pressure reduction from that required at the asymptotic limit. The CP layer fully develops toward its asymptotic limit after τ exceeds $1/2$, especially for higher rejections.

2.10. Effects of pressure release

Fig. 6 shows the initial growth of the $\phi_m(\tau)$ of Eq. (59) from $\tau = 0$ to the permeation–stopping time at (a) $\tau_s = 2$ and (b) $\tau_s = 4$ for several R_o values. In both τ_s cases, ϕ_m trends are similar before and after τ_s. The dash-dot line in Fig. 1 is identical to $\phi_m(0 < \tau < 2, R_o = 1)$ in Fig. 6(a) and (b). During the initial period of $\tau < 1/2$, nonlinear behaviors are established, which trigger linear asymptotic behaviors until the pressure is released at $\tau = \tau_s$. During the permeation period $(0 < \tau < \tau_s)$, solutes are continuously brought down toward the membrane surface through fixed permeation, and the interfacial concentration increases steadily after $\tau \langle 1/2)$. The movement of molecules toward the membrane surface is influenced by the constant permeation flux forming the CP layer and the back diffusion caused by the CP phenomenon. The time scale of the

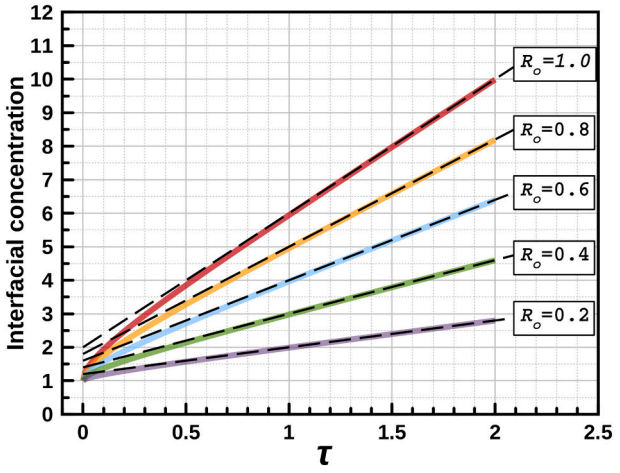

Fig. 4. The interfacial concentrations of $\phi_m(\tau, R)$ with time τ for rejection ratio R_o from 0.2 to 1.0 (semi-transparent solid lines) and their asymptotic limits (dashed lines).

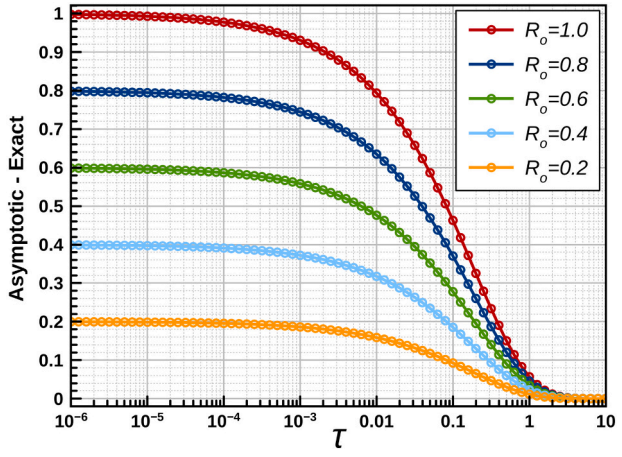

Fig. 5. Differences between the asymptotic and exact functional forms of $\phi_m(\tau)$ with time τ for rejection ratio R_o from 0.2 to 1.0. For the perfect rejection $R_o = 1$, errors between ϕ^* and ϕ_m are 15.3 % at $\tau = 0.5$ and 5.68 % at $\tau = 1$.

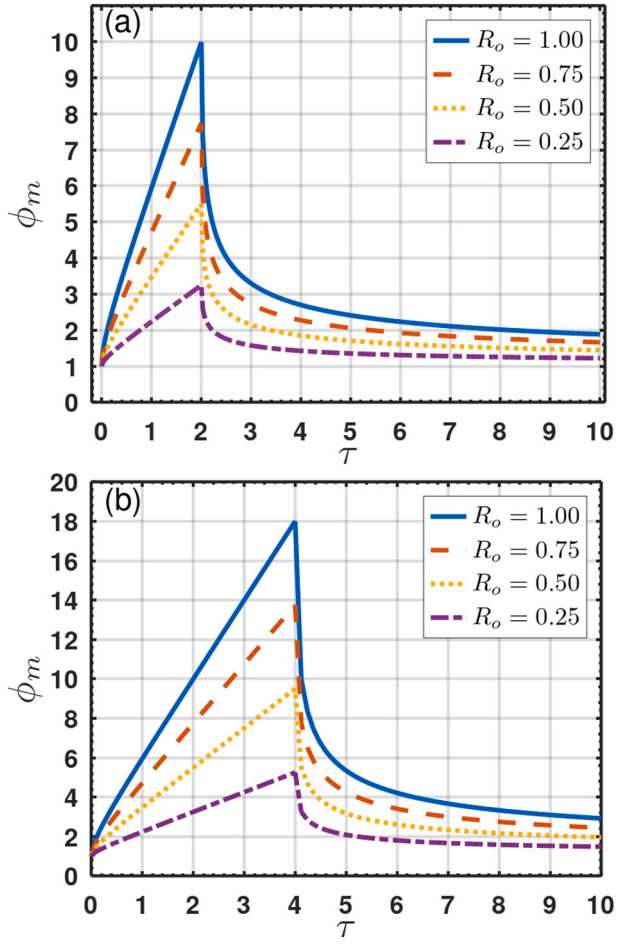

Fig. 6. The growth of interfacial concentration $\phi_m(\tau)$ with time τ for $\tau \le \tau_s$ and decline for $\tau > \tau_s$ with various observed rejection values: (a) $\tau_s = 2$ and (b) $\tau_s = 4$.

dead-end filtration process is much longer (e.g., of an order of 10 min) than the molecular relaxation time. Therefore, the filtration system can be considered in equilibrium at the molecular level. At a given time τ, while solutes are rejected on the membrane surface, the concentration decreases exponentially with respect to the distance from the membrane surface η, as implied in Eq. (70). The net mass transport rate per membrane surface area at any given time τ equals the feed input rate of $C_f J_w$, determined far from the membrane surface. For a high rejection ratio, i.e., $R_o \to 1$, the accumulation rate can be close to the feed input rate.

Once the transmembrane pressure is released at $\tau = \tau_s$, $\phi_m(\tau)$, the value of $\phi_m(\tau)$ decreases from its peak value described in Eq. (79) to the ultimate value of 1, which reduces the degree of the CP. However, in the absence of permeation, the sole back-diffusion does not bring the concentration profile back to its initial stage of $\phi(\eta, \tau) = 1$, and even after a long time, $\phi_m(\tau)$ remains at 1. The initial concentration declines immediately after the stopping times in Fig. 6(a) and (b) are visually estimated, such as from $\phi_m(\Delta\tau = 0, R_o = 1) \simeq 10$ to $\phi_m(\Delta\tau = 1, R_o = 1) \simeq 3.4$ for $\tau_s = 2$ and from $\phi_m(\Delta\tau = 0, R_o = 1) \simeq 18$ to $\phi_m(\Delta\tau = 1, R_o = 1) \simeq 5.2$ for $\tau_s = 4$, respectively. A rough estimation of the concentration decrease rates gives $\Delta\phi_m/\Delta\tau \simeq 6.6$ for $\tau_s = 2$ and $\Delta\phi_m/\Delta\tau \simeq 12.8$ for $\tau_s = 4$. A longer filtration time provides a higher interfacial concentration and a faster diffusion rate but requires a longer time to reach a desired concentration to restart the dead–end filtration. As a result, the concentration gradient will persist as long as the decreasing interfacial concentration reduces the back diffusion as a driving force.

A permeation restarting time can be determined when the interfacial concentration reaches a limit, denoted as ϕ_{lim}, that is approaching to 1 from ϕ_{max}. We define a new time scale, denoted as $\Delta\tau$, i.e., the time required for ϕ_m to decrease from ϕ_{max} at τ_s to a specific ϕ_{lim} at $\tau_s + \Delta\tau$; and calculate $\Delta\tau$ as a function of ϕ_{max} and ϕ_{lim}, using

$$e^{x^2}\, erfc(x) = \frac{\varphi_{\text{lim}} - 1}{\phi_{\text{max}} - 1} \tag{111}$$

derived from Eq. (80), where $x = \beta\sqrt{\Delta\tau}$ and $\beta = 2$. Fig. 7 shows how $\Delta\tau$ varies with specified ϕ_{lim} with respect to ϕ_{max}. In the asymptotic limit of $\tau > 1/2$, one can calculate ϕ_m^* at $\tau = \tau_s$ as ϕ_{max} using Eq. (100), such as

$$\phi_{\text{max}} \simeq 1 + R_o(1 + 4\tau_s) \tag{112}$$

and estimate an approximate elapsed time $\Delta\tau$ to reach ϕ_{lim} by visually investigating Fig. 7. As expected, a high value of $\phi_{\text{lim}} = 2.0$ takes the shortest time to reach, followed by 1.75 and other smaller values. The lowest values of $\phi_{\text{lim}} = 1.25$ in Fig. 7 require $\Delta\tau$ at least one order–of–magnitude higher than τ_s, especially when $\phi_{\text{max}} > 4$. The present analysis of $\Delta\tau$ quantitatively confirms that the periodic pressure release does not return the filtration system to the initial stage having the constant, lowest uniform concentration of C_f. The complete removal of the concentration polarization requires other external processes such as backflushing (depending on solute and membrane types), sweeping, or

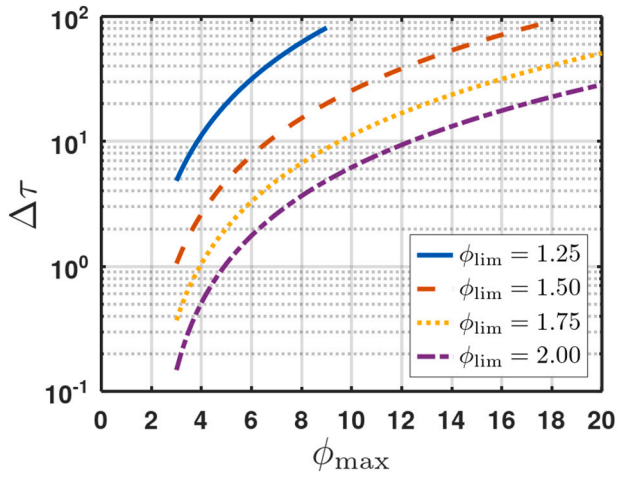

Fig. 7. The dimensionless duration $\Delta\tau$ to reach the limiting concentration ϕ_{lim} form the maximum concentration ϕ_{max} reached when the filtration stops.

stirring, in principle.

Fig. 7 shows how $\Delta\tau$ varies with specified $\phi_{\lim}$ with respect to $\phi_{\max}$. In the asymptotic limit of $\tau > 1/2$, one can calculate ϕ_m^* at $\tau = \tau_s$ as $\phi_{\max}$ using Eq. (100), such as

$$\phi_{\max} \simeq 1 + R_o(1 + 4\tau_s) \tag{113}$$

and estimate an approximate elapsed time $\Delta\tau$ to reach a specific value of $\phi_{\lim}$ by visually investigating Fig. 7. As expected, a high value of $\phi_{\lim} = 2.0$ takes the shortest time to reach from a given $\phi_{\max}$, followed by 1.75 and other smaller values. The lowest values of $\phi_{\lim} = 1.25$ in Fig. 7 require $\Delta\tau$ at least one order–of–magnitude higher than τ_s, especially when $\phi_{\max} > 4$. The present analysis of $\Delta\tau$ quantitatively confirms that the periodic pressure release does not return the filtration system to the initial stage of the constant, lowest uniform concentration of C_f. The complete removal of the concentration polarization requires other external processes such as backflushing (depending on solute and membrane types), sweeping, or stirring, in principle.

3. Concluding remarks

This study revisits the fundamental dead-end filtration theory for constant–flux operation and develops a complete analytic solution of Eq. (59) for the interface concentration as a function of filtration time τ and observed rejection ratio R_o. The current theory does not employ physical assumptions, mathematical approximations, or empirical parameters. The presence of a convection term creates formidable complexity in developing analytic solutions for the spatiotemporal profile of a solute concentration, due to a lack of the inverse Laplace transform formulae for functions containing the $\sqrt{p+1}$ term. To analytically solve for the interfacial concentration $\phi_m(\tau)$, we use several tabulated formulae of the Laplace transform, containing the error function (erf) and complementary error function (erfc), combine the necessary inverse Laplace transforms, and use the convolution theorem to finish the inverse Laplace transform.

The asymptotic limit of the analytic solution indicates that the interfacial concentration rate $\dot{\phi}_m$ reaches $4R_o$, implying that the hydraulic pressure requirement is also proportional to a product of τ and R_o, i.e., $\phi_m \propto 4R_o\tau$. The analytic solution for $\phi_m(\tau)$ is reversely validated by numerical solutions, obtained by the most error–vulnerable forward scheme. Because implementing the boundary condition on the membrane surface requires an accurate estimation of the concentration gradient, the stiff slope of the spatial concentration profile mandates using multiple–point differentiation. The elapsed time to reach a specific limiting concentration $\phi_{\lim}$ below 2 is calculated using the analytical solution developed in this study, as a function of $\phi_{\lim}$ and the permeation stopping time τ_s. The present theoretical analysis using the derived analytical solution provides clear insight into the constant–flux dead-end filtration, an in-depth understanding of the interfacial concentration as an essential component to estimate the spatial concentration polarization, and a solid foundation to pursue the full spatiotemporal profile of concentration within the polarization layer. The mathematical method based on the Laplace transform and convolution theorem can contribute to solving challenging problems of membrane separation with or without stirring in both continuous and syringe-type feeding for constant-flux and constant-pressure operations.

CRediT authorship contribution statement

Albert S. Kim: Conceptualization, Methodology, Software, Validation, Formal analysis, Investigation, Resources, Writing – original draft, Writing – review & editing, Visualization, Funding acquisition.

Declaration of competing interest

The authors declare that they have no known competing financial interests or personal relationships that could have appeared to influence the work reported in this paper.

Data availability

No data was used for the research described in the article.

Acknowledgments

This work has been supported in part by the U.S. National Science Foundation (grant no. 2034824).

Appendix A

A.1. Approximation of error function

In principle, evaluation of the error function requires numerical integration, although most modern programming languages have the error function embedded for users to call on. However, a good approximation of the error function is given as

$$erf(x) \simeq tanh\left(ax + bx^3\right) \tag{A.1}$$

where $a = 167/148$ and $b = 11/109$ with the absolute difference of an order of $O\left(10^{-4}\right)$ [31]. An alternative value of $a = 123/109$ is suggested to have the same denominator with b with the same error range.

A.2. Non–iterative numerical procedure

The dimensionless concentration $\phi(\tau, \eta)$ is discretized using the standard scheme as $\phi_{j,k}$ for τ–index $j = 1 - M$ and η–index $k = 1 - N$, such as

$$\frac{\phi_{j+1,k} - \phi_{j,k}}{\delta\tau} = \frac{\phi_{j,k+1} - 2\phi_{j,k} + \phi_{j,k-1}}{(\delta\eta)^2} + 2\lambda\frac{\phi_{j,k+1} - \phi_{j,k-1}}{2\delta\eta} \tag{A.2}$$

resulting in the $\phi(\eta = k\delta\eta)$ at the next time step $j + 1$, such as

$$\phi_{j+1,k} = \phi_{j,k} + \left(\phi_{j,k+1} - 2\phi_{j,k} + \phi_{j,k-1}\right)\frac{\delta\tau}{(\delta\eta)^2} + \lambda\left(\phi_{j,k+1} - \phi_{j,k-1}\right)\frac{\delta\tau}{\delta\eta} \tag{A.3}$$

The initial and far–field boundary conditions of Eqs. (19) and (20) are applied, such as

$$\phi(0,\eta)\rightarrow\phi_{1,k}=1 \quad \text{for all } k \tag{A.4}$$

$$\phi(\tau,\infty)\rightarrow\phi_{j,N}=1 \quad \text{for all } j \tag{A.5}$$

respectively, and the interfacial condition (at $\eta = 0$) is given as

$$\left[\frac{\partial\phi}{\partial\eta}\right]_{k=1} = -f\left(\phi_{j,1}-\phi_p\right) \tag{A.6}$$

We discretized the interfacial gradient of ϕ using 2, 3, and 5 point–schemes, such as

$$\left[\frac{\partial\phi}{\partial\eta}\right]^{[2]}_{\eta=0} = \frac{\phi_{j2}-\phi_{j1}}{\delta\eta} \tag{A.7}$$

$$\left[\frac{\partial\phi}{\partial\eta}\right]^{[3]}_{\eta=0} = \frac{-3\phi_{j1}+4\phi_{j2}-\phi_{j3}}{2\delta\eta} \tag{A.8}$$

$$\left[\frac{\partial\phi}{\partial\eta}\right]^{[5]}_{\eta=0} = \frac{-25\phi_{j1}+48\phi_{j2}-36\phi_{j3}+16\phi_{j4}-3\phi_{j5}}{12\delta\eta} \tag{A.9}$$

where the numbers in the squared brackets of the superscripts indicate the number of points used for differentiation. For numerical stability, we restrict simulations for

$$\frac{\delta\tau}{(\delta\eta)^2}\le 1 \quad \text{and} \quad \frac{\delta\tau}{\delta\eta}\le 1 \tag{A.10}$$

where the first condition will automatically satisfy the second condition because both $\delta\tau$ and $\delta\eta$ are less than 1, which is re–written as

$$\frac{\delta\tau}{(\delta\eta)^2} = \frac{\tau_{\max}}{M}\frac{N^2}{\eta^2_{\max}} = \frac{\tau}{\eta^2_{\max}}\frac{N^2}{M} \tag{A.11}$$

The following conditions are used to unconditionally satisfy the numerical convergence, such as: $M = N^2$ and

$$\frac{\tau_{\max}}{\eta^2_{\max}} < 1 \tag{A.12}$$

We find that $N = 10^3$ is a reasonable value and use $\tau_{\max} = 2$ and $\eta_{\max} = 4$ to confirm $\tau_{\max}/\eta^2_{\max} = 2/4^2 = 1/8 = 0.125 < 1$. For other cases of $\tau_{\max}$, $\eta_{\max}$ is proportionally determined. The sequential steps of the finite difference method simulation are as follows.

1. Using the parameters of $\tau_{\max}$, $\eta_{\max}$, M, and N, calculate the spatial and temporal intervals, $\delta\eta$ and $\delta\tau$, respectively.
2. Let $\phi_{j,k} = 1$ for all $j = 1 - M$ and $k = 1 - N$, which automatically assign the initial and far–field boundary conditions, i.e., $\phi_{1,k} = 1$ and $\phi_{j,N} = 1$, respectively.
3. Using $\phi_{j,k}$ known for the current time step j,
   (a) calculate $\phi_{j+1,k}$ for k from $N - 1$ to 2, and
   (b) calculate the interfacial concentration $\phi_{j+1,1}$ using one of the differentiation schemes.
4. Go to the next time step until j reaches the maximum time index M.

The dimensionless maximum $\tau_{\max}$ should be long enough to observe asymptotic behavior of the interfacial concentration for a long term, and the dimensionless maximum length $\eta_{\max}$ should be long enough to apply the far–field boundary condition of Eq. (20) in either Dirichlet or Neumann form.

References

[1] E. Drioli, A. Criscuoli, E. Curcio, Membrane contactors: fundamentals, applications and potentialities, in: Membrane Science and Technology Series, 1st edition, Elsevier, Amsterdam; Boston, 2006 (no. 11).

[2] M. Mulder, Basic Principles of Membrane Technology, Springer Netherlands, Dordrecht, 1996, https://doi.org/10.1007/978-94-009-1766-8.

[3] Membrane separations technology: principles and applications, in: R.D. Noble, S. A. Stern (Eds.), Membrane Science and Technology Series, Elsevier, Amsterdam; New York, 1995 (no. 2).

[4] M. Weiss, R. Ruess, J. Kasnatscheew, Y. Levartovsky, N.R. Levy, P. Minnmann, L. Stolz, T. Waldmann, M. Wohlfahrt-Mehrens, D. Aurbach, M. Winter, Y. Ein-Eli, J. Janek, Fast charging of lithium-ion batteries: a review of materials aspects, Adv. Energy Mater. 11 (33) (2021), 2101126, https://doi.org/10.1002/aenm.202101126.

[5] C. Shang, J. Xia, L. Sun, G.G. Lipscomb, S. Zhang, Concentration polarization on surface patterned membranes, AICHE J. 68 (12) (2022), e17832, https://doi.org/10.1002/aic.17832.

[6] C.-Y. Lin, C. Combs, Y.-S. Su, L.-H. Yeh, Z.S. Siwy, Rectification of concentration polarization in mesopores leads to high conductance ionic diodes and high performance osmotic power, J. Am. Chem. Soc. 141 (8) (2019) 3691–3698, https://doi.org/10.1021/jacs.8b13497.

[7] W. Han, X. Chen, A review: applications of ion transport in micro-nanofluidic systems based on ion concentration polarization, J. Chem. Technol. Biotechnol. 95 (6) (2020) 1622–1631, https://doi.org/10.1002/jctb.6288.

[8] W. Bai, L. Samineni, P. Chirontoni, I. Krupa, P. Kasak, A. Popelka, N.B. Saleh, M. Kumar, Quantifying and reducing concentration polarization in reverse osmosis systems, Desalination 554 (2023) 116480, https://doi.org/10.1016/j.desal.2023.116480.

[9] A. Imbrogno, A.I. Schäfer, Comparative study of nanofiltration membrane characterization devices of different dimension and configuration (cross flow and dead end), J. Membr. Sci. 585 (2019) 67–80, https://doi.org/10.1016/j.memsci.2019.04.035.

[10] U.M. Aliyu, S. Rathilal, Y.M. Isa, Membrane desalination technologies in water treatment: a review, Water Pract. Technol. 13 (4) (2018) 738–752, https://doi.org/10.2166/wpt.2018.084.

[11] J. Crank, The Mathematics of Diffusion, 2nd edition, Clarendon Press, Oxford [Eng], 1975.

[12] H.S. Carslaw, J.C. Jaeger, Conduction of Heat in Solids, 2nd edition, Clarendon, Oxford, 1980.

[13] M.F.N. Mohsen, M.H. Baluch, An analytical solution of the diffusion- convection equation over a finite domain, Appl. Math. Model. 7 (4) (1983) 285–287, https://doi.org/10.1016/0307-904X(83)90084-7.
[14] X. Guo, Z. Chai, S. Pang, Y. Zhao, B. Shi, Mixed bounce-back boundary scheme of the general propagation lattice Boltzmann method for advection-diffusion equations, Phys. Rev. E 99 (6) (2019), 063316, https://doi.org/10.1103/PhysRevE.99.063316.
[15] A.R. Ansari, A.F. Hegarty, Numerical solution of a convection diffusion problem with Robin boundary conditions, J. Comput. Appl. Math. 156 (1) (2003) 221–238, https://doi.org/10.1016/S0377-0427(02)00913-5.
[16] K. Gustafson, T. Abe, The third boundary condition— was it robin's? Math. Intell. 20 (1) (1998) 63–71, https://doi.org/10.1007/BF03024402.
[17] A.S. Kim, Complete analytic solutions for convection-diffusion-reaction-source equations without using an inverse Laplace transform, Sci. Rep. 10 (1) (2020) 8040, https://doi.org/10.1038/s41598-020-63982-w.
[18] A.S. Kim, Permeate flux inflection due to concentration polarization in crossflow membrane filtration: a novel analytic approach, Eur. Phys. J. E 24 (4) (2007) 331, https://doi.org/10.1140/epje/i2007-10244-x.
[19] M.L. Boas, Mathematical Methods in the Physical Sciences, Wiley, Hoboken, NJ, 2006.
[20] M.-S. Chun, W.C. Park, Time evolution of electrokinetic flow-induced streaming potential and flux in dead-end and cross-flow filtration of colloids through nanopores, J. Membr. Sci. 243 (1) (2004) 417–424, https://doi.org/10.1016/j.memsci.2004.07.009.
[21] T.C. Arnot, R.W. Field, A.B. Koltuniewicz, Cross-flow and dead-end microfiltration of oily-water emulsions: part II. Mechanisms and modelling of flux decline, J. Membr. Sci. 169 (1) (2000) 1–15, https://doi.org/10.1016/S0376-7388(99)00321-X.
[22] L. Dresner, Boundary Layer Built-up in the Demineralization of Salt Water by Reverse Osmosis, Technical Report ORNL-3621, Neutron Physics Division, Oak Ridge National Laboratory, 1964.
[23] R.J. Raridon, L. Dresner, K.A. Kraus, Hyperfiltration studies V. Salt rejection of membranes by a concentration polarization method, Desalination 1 (3) (1966) 210–224, https://doi.org/10.1016/S0011-9164(00)80253-2.
[24] H. Kramers, G. Alberda, Frequency response analysis of continuous flow systems, Chem. Eng. Sci. 2 (4) (1953) 173–181, https://doi.org/10.1016/0009-2509(53)80039-4.
[25] P.V. Danckwerts, Continuous flow systems: distribution of residence times, Chem. Eng. Sci. 2 (1) (1953) 1–13, https://doi.org/10.1016/0009-2509(53)80001-1.
[26] J.F. Wehner, R.H. Wilhelm, Boundary conditions of flow reactor, Chem. Eng. Sci. 6 (2) (1956) 89–93, https://doi.org/10.1016/0009-2509(56)80014-6.
[27] H.K. Lonsdale, U. Merten, R.L. Riley, Transport properties of cellulose acetate osmotic membranes, J. Appl. Polym. Sci. 9 (4) (1965) 1341–1362, https://doi.org/10.1002/app.1965.070090413.
[28] J.G. Wijmans, R.W. Baker, The solution-diffusion model: a review, J. Membr. Sci. 107 (1) (1995) 1–21, https://doi.org/10.1016/0376-7388(95)00102-I. URL. https://www.sciencedirect.com/science/article/pii/037673889500102I.
[29] W.M. Haynes (Ed.), CRC Handbook of Chemistry and Physics: A Ready-reference Book of Chemical and Physical Data, 95th edition, CRC Press, Boca Raton London New York, 2014.
[30] A.V.M. Polyanin Polyanin, Handbook of integral equations, in: Handbook of Integral Equations, second edition, CRC Press, London, 2008.
[31] J.D. Vedder, Simple approximations for the error function and its inverse, Am. J. Phys. 55 (8) (1987) 762–763, https://doi.org/10.1119/1.15018.
[32] Y. Nakano, C. Tien, W.N. Gill, Nonlinear convective diffusion: a hyperfiltration application, AICHE J. 13 (6) (1967) 1092–1098, https://doi.org/10.1002/aic.690130611. URL, https://onlinelibrary.wiley.com/doi/10.1002/aic.690130611.
[33] F.A. Williams, A nonlinear diffusion problem relevant to desalination by reverse osmosis, SIAM J. Appl. Math. 17 (1) (1969) 59–73, https://doi.org/10.1137/0117006. URL, http://epubs.siam.org/doi/10.1137/0117006.
[34] M.K. Liu, F.A. Williams, Concentration polarization in an unstirred batch cell: measurements and comparison with theory, Int. J. Heat Mass Transf. 13 (9) (1970) 1441–1457, https://doi.org/10.1016/0017-9310(70)90179-1.
[35] S. Bouranene, P. Fievet, A. Szymczyk, M. El-Hadi Samar, A. Vidonne, Influence of operating conditions on the rejection of cobalt and lead ions in aqueous solutions by a nanofiltration polyamide membrane, J. Membr. Sci. 325 (1) (2008) 150–157, https://doi.org/10.1016/j.memsci.2008.07.018. URL, https://linkinghub.elsevier.com/retrieve/pii/S0376738808006716.